Optics Communications 418 (2018) 129–134

Contents lists available at ScienceDirect

Optics Communications

journal homepage: www.elsevier.com/locate/optcom

Adaptive inversion algorithm for 1.5 μm visibility lidar incorporating in situ Angstrom wavelength exponent

Xiang Shang, Haiyun Xia *, Xiankang Dou, Mingjia Shangguan, Manyi Li, Chong Wang

CAS Key Laboratory of Geospace Environment, USTC, Hefei, 230026, China
School of Earth and Space Sciences, USTC, Hefei, 230026, China

ARTICLE INFO

Keywords:
Visibility lidar
Aerosol size distribution
Angstrom wavelength exponent

ABSTRACT

An eye-safe 1.5 μm visibility lidar is presented in this work considering in situ particle size distribution, which can be deployed in crowded places like airports. In such a case, the measured extinction coefficient at 1.5 μm should be converted to that at 0.55 μm for visibility retrieval. Although several models have been established since 1962, the accurate wavelength conversion remains a challenge. An adaptive inversion algorithm for 1.5 μm visibility lidar is proposed and demonstrated by using the in situ Angstrom wavelength exponent, which is derived from an aerosol spectrometer. The impact of the particle size distribution of atmospheric aerosols and the Rayleigh backscattering of atmospheric molecules are taken into account. Using the 1.5 μm visibility lidar, the visibility with a temporal resolution of 5 min is detected over 48 h in Hefei (31.83 °N, 117.25 °E). The average visibility error between the new method and a visibility sensor (Vaisala, PWD52) is 5.2% with the R-square value of 0.96, while the relative error between another reference visibility lidar at 532 nm and the visibility sensor is 6.7% with the R-square value of 0.91. All results agree with each other well, demonstrating the accuracy and stability of the algorithm.

1. Introduction

Almost all places where visibility needs to be detected have a lot of people. Thus, the eye safety is an important problem that must be considered when measuring visibility in crowded places like airports. Visibility is of decisive importance for all kinds of traffic operations and air pollution monitoring [1]. Visibility can also directly reflect the atmospheric turbidity [2]. In the free-space optical (FSO) communication systems, visibility can be used to estimate its availability performance [3]. According to Koschmieder's theory, visibility is directly related to the extinction coefficient at 0.55 μm and to the contrast threshold of an observer who needs to distinguish an object from its background [4]. The traditional visibility sensors can be divided into two types. One is transmissometer, which is fixed installations for the determination of optical transmission between two locations. The other is scatter visibility sensor, which is an in situ device determining visibility in one point. Unlike traditional visibility sensors, lidar measures atmospheric backscattering to retrieve the visibility. It makes observations of atmospheric conditions over an extended optical path from one location, in any, not just in horizontal direction [2].

Lidar systems can make atmospheric observations at different wavelengths ranging from UV to NIR (such as 355 nm, 532 nm and 1064 nm) [5–7]. Recently, the 1.5 μm lidar has been recognized as an important instrument in multifrequency lidar systems for the measurements of PM10 [8], since it detects the Mie backscattering at longer wavelength than those systems mentioned above. By using the stimulated Raman scattering in methane, a transmitter that produces a high-pulse-energy laser at 1.5 μm is adopted to develop a direct analog-detection lidar, which has been used for the observation of wind and plumes from aerosol generators [9–11]. The extinction values derived from a 1.55 μm laser rangefinder are used to assist active and passive electro-optical sensor's performance prediction in low visibility conditions [12]. The first micropulse lidar is developed by J. D. Spinhirne in 1993 [13]. Recently, a micropulse 1.5 μm aerosol lidar is demonstrated to measure the atmospheric parameters in Hefei, China [14].

There are some advantages to monitoring visibility at 1.5 μm than at UV and visible wavelengths, including the highest maximum permissible exposure to human eyes [15], lower signal contribution from Rayleigh backscattering, weaker sky radiance and lower atmospheric attenuation [16]. Due to the advantage of eye-safe, the 1.5 μm visibility lidar is suitable to be applied in crowded places. Furthermore, 1.5 μm is a standard wavelength of optical telecommunications, optical fiber components and devices are commercial available [17], reducing

* Corresponding author at: School of Earth and Space Sciences, USTC, Hefei, 230026, China.
E-mail address: hsia@ustc.edu.cn (H. Xia).

https://doi.org/10.1016/j.optcom.2018.03.009
Received 9 January 2018; Received in revised form 2 March 2018; Accepted 5 March 2018

the cost in constructing a lidar system substantially. Finally, thanks to the lowest attenuation in the optical fiber at 1.5 μm, an all-fiber integrated system offers unparalleled features in field experiments, such as mechanical decoupling and remote installation of the subsystems, simplification of optical configuration and alignment, enhancement in coupling efficiency and long-term stability [18].

But, the visibility is commonly defined at 0.55 μm, the most sensitive wavelength for human eyes. So, all the measured atmospheric extinction coefficients at other wavelengths should be converted to the extinction coefficient at 0.55 μm. From 1960s, great efforts have been devoted to this issue. A semi-empirical three-stage formula, called the Kruse formula, is typically used to determine the wavelength dependence of the atmospheric extinction coefficient, and it is the only model providing a wavelength dependent relation between the atmospheric visibility and the extinction coefficient during a long time [19]. At the beginning of the 21st century, Kim indicated that the Kruse formula did not have a good performance in fog conditions. On the basis of the Kruse formula, Kim gave a five-stage function [20]. Later, Naboulsi considered two specific weather conditions, advection fog and convection fog, with experimental data measured on the site La Turbie at Nice, France [21]. By taking the radius of scatterers into account, Grabner analyzed the wavelength dependence using Mie scattering theory and proposed a new model [22]. However, the wavelength dependences are different in these models, because they have to assume the characteristics of the atmospheric particles at the location of their experiment. The aerosol's microphysical properties vary significantly and fast in time and space, making the determination of the wavelength dependence to be a complex problem [23]. The particles in the atmosphere can be divided to biomass burning aerosol, dust, etc. For different kind of particles, the wavelength dependence is different.

A convenient way to convert extinction coefficients between different wavelengths is using Angstrom exponent derived from aerosol optical depth [24–26], which is defined as the integration of extinction coefficient along the entire atmospheric column vertically. The aerosol optical depth can be obtained from measurement of sun photometer or satellite remote sensing. A high-precision multiband sun photometer measures the optical properties of the atmosphere based on the sun irradiance and the sky radiance. It provides the quantification and physical–optical characterizations of the aerosols. In an atmospheric correction model, with assumed vertical structure of the atmosphere, aerosol optical depth shown a relation with the meteorological visibility measured horizontally at the surface [27]. The sun photometer can only be used during daytime, which cannot meet the needs of day and night observation of visibility lidar.

In this work, an adaptive inversion algorithm for a 1.5 μm visibility lidar is proposed. The Angstrom wavelength exponent is retrieved from the particle size distribution (PSD) measured by an aerosol spectrometer (Grimm, 11-R). In the experiment, in order to test the accuracy of the algorithm, we compared the extinction coefficients measured by a reference lidar at 532 nm and the 1.5 μm lidar. Finally, the visibility measured by 1.5 μm lidar is compared with a commercial available visibility sensor (Vaisala, PWD50), demonstrating the correctness and accuracy of the new algorithm.

2. Principle

The lidar equation is given as:

$$N(R) = E\eta_0 \frac{\eta_q}{h\nu} \frac{A}{R^2} O(R) \frac{c\Delta t}{2} \beta(R) \exp\left[-2\int_0^r \sigma(R')dR'\right], \tag{1}$$

where $N(R)$ is the number of photons backscattered from the range R, E is the energy of the laser pulse, η_0 accounts for the optical efficiency of the system, η_q is the quantum efficiency of the detector, h is the Planck constant, ν is the frequency of the photon, A is the receiver area of the telescope, R is the range from the lidar to the scattering volume, $O(R)$ is the laser-beam receiver-field-of-view overlap function, c is the speed of light, Δt is the duration of the laser pulse, β and σ are the atmospheric backscatter coefficient and atmospheric extinction coefficient, respectively.

If the atmosphere is homogeneous and β does not change with R, the extinction coefficient can be expressed as [28]:

$$\sigma = -\frac{1}{2}\frac{d\ln[R^2N(R)]}{dR}. \tag{2}$$

Commonly, by assuming a constant ratio between $\sigma(R)$ and $\beta(R)$, the inversion algorithm proposed by Klett and Fernald can be used to retrieve $\sigma(R)$ [29,30]. Considering the experiment conditions in this work, there are two reasons for using Eq. (2) to get the extinction coefficient at 1.5 μm. Firstly, when measuring the visibility, the laser is emitted horizontally and the lidar is installed on the top of our building, with a height of 56 m above the ground. As shown in Fig. 3, the lidar signal decreases smoothly. Secondly, the correlation coefficient of the linear fitting of Eq. (2) is 1 if the atmosphere is completely homogeneous. During the data processing of this work, the range interval of the original data is shifted slightly to make sure the correlation coefficient is greater than 0.95.

According to Koschmieder's theory, visibility is expressed as [4]:

$$V = \frac{1}{\sigma}\ln\frac{1}{K} \approx \frac{3}{\sigma_0}, \tag{3}$$

where the contrast threshold K is chosen as 0.05 and the extinction coefficient σ is taken at $\lambda_0 = 550$ nm. In the practical application of 1.5 μm visibility lidar, the measured atmospheric extinction coefficients at $\lambda_1 = 1548$ nm should be converted to the extinction coefficient at 550 nm to calculate visibility.

The extinction coefficient σ'_λ due to Mie scattering of aerosol particles can be calculated as:

$$\sigma'_\lambda = \int_{r_{\min}}^{r_{\max}} \pi r^2 Q_{ext}\left[r, \lambda, m^*_\lambda\right] n(r)dr, \tag{4}$$

where r is the particle's radius, Q_{ext} is the extinction efficiency factor, m^*_λ is the complex refractive index at wavelength λ, the particle size distribution $n(r)$ is the number of particles per unit volume in the interval $(r, r+dr)$. For a given wavelength λ, there are only two unknowns $n(r)$ and m^*_λ in Eq. (4).

When $n(r)$ is measured by aerosol spectrometer and the refractive index is an empirical value, σ'_0 and σ'_1 can be calculated using Eq. (4). Then, the Angstrom wavelength exponent can be calculated as:

$$\alpha_1 = -\frac{\ln(\sigma'_0/\sigma'_1)}{\ln(\lambda_0/\lambda_1)}. \tag{5}$$

As an example, the Q_{ext} is calculated using Mie scattering theory when $m^*_\lambda = 1.33$, as shown in Fig. 1(a). Two typical PSDs of Hefei (31.83°N, 117.25°E) are shown in Fig. 1(b). The σ'_λ calculated by Eq. (4) and α_1 calculated by Eq. (5) are shown in Fig. 1(c). A bimodal lognormal distribution is used to fit the PSD raw data:

$$\begin{aligned} n(r) = {} & \frac{C_1}{\sqrt{2\pi}\delta_1 r}\exp\left[-\frac{(\ln r - \ln R_1)^2}{2\delta_1^2}\right] \\ & + \frac{C_2}{\sqrt{2\pi}\delta_2 r}\exp\left[-\frac{(\ln r - \ln R_2)^2}{2\delta_2^2}\right], \end{aligned} \tag{6}$$

where C_1, δ_1, R_1, C_2, δ_2, R_2 are fitting parameters of the bimodal lognormal distribution. The volume size distribution is also widely used in the atmospheric researches. It is defined as:

$$dV/d\log(r) = \frac{4}{3}\pi r^3 n(r)dr/d\log(r). \tag{7}$$

Using the atmospheric extinction coefficient σ_1 obtained by Eq. (2) and the Angstrom wavelength exponent α_1 obtained by Eq. (5), σ_0 is calculated as:

$$\sigma_0 = \sigma_1(\lambda_1/\lambda_0)^{\alpha_1}. \tag{8}$$

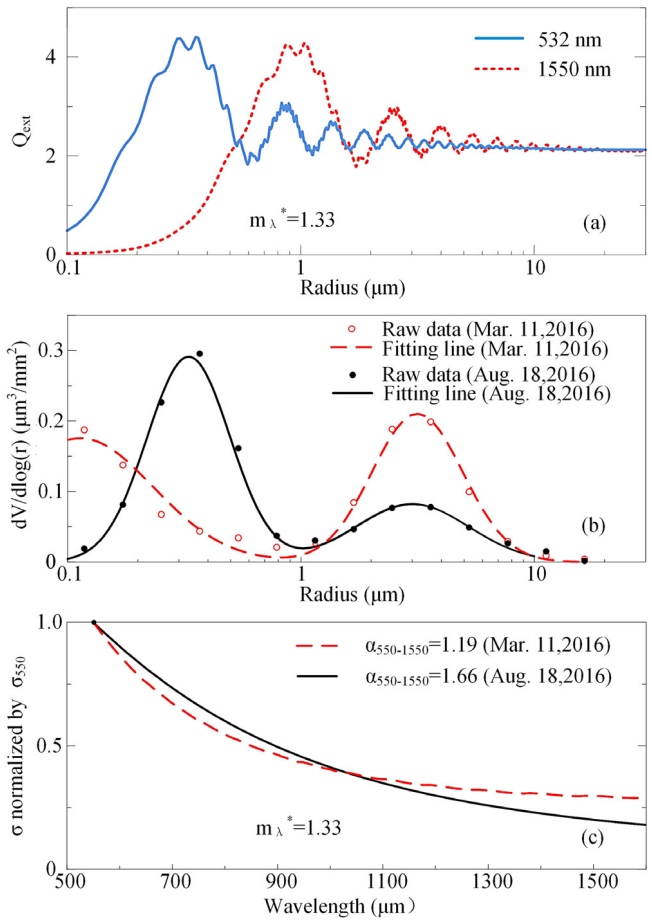

Fig. 1. The extinction efficiency factors of 532 nm and 1.55 μm (a), two types of typical bimodal lognormal size distributions in Hefei (b), and normalized extinction coefficients (c).

The visibility can be calculated by:

$$V = \frac{3}{\sigma_0} = \frac{3}{\sigma_1}(\lambda_1/\lambda_0)^{-\alpha_1}. \tag{9}$$

The sun photometer can also retrieve α_1 from the AOD, but it is a passive detection instrument with lower time resolution than aerosol spectrometer. It can only be used during daytime and is affected by the weather conditions. Thus, aerosol spectrometer is used in this work.

It is important to note that the wavelength dependence of molecular Rayleigh scattering is different from aerosol Mie scattering [31]. The molecular Rayleigh extinction coefficient $\sigma_{R,\lambda}$ is approximated as [32]:

$$\sigma_{R,\lambda} = \frac{9.807}{10^{20}}\frac{273}{T}\frac{P}{1013}\left(\frac{10^7}{\lambda}\right)^{4.0117}, \tag{10}$$

where T and P are the atmospheric temperature and pressure, respectively. As Rayleigh extinction is considered, Eq. (9) should be updated to calculate the atmospheric visibility:

$$V = \frac{3}{(\sigma_1 - \sigma_{R,1})(\lambda_1/\lambda_0)^{\alpha_1} + \sigma_{R,0}}. \tag{11}$$

3. Instrument

The 1.5 μm lidar system used in this experiment has been described in detail elsewhere for aerosol and wind detection [14,18]. A brief review is given here. The lidar operating at 1.5 μm ensures the eye safety of human beings, so that the experiment can be performed in urban areas. As detectors are considered, InGaAs/InP avalanche photodiode is used for 1.5 μm detection commonly, but it suffers low efficiency (about 10%), high dark count noise (a few kHz) and high after pulsing possibility (18%) [33]. To solve this problem, an up-conversion detector (UCD) is used in this experiment. The UCD up-converts photons at 1.55 μm to 863 nm in a periodically poled lithium niobate waveguide (PPLN-W). Then single photon at 1.55 μm can be counted by using a Si: APD with high efficiency (20%), low dark count noise (300 Hz) and negligible after pulsing possibility (0.2%) [34,35].

Table 1
Key parameters of the visibility lidars.

Parameter	1.5 μm lidar	532 nm lidar
Wavelength (nm)	1548	532
Pulse duration (ns)	300	7
Pulse energy (mJ)	0.11	15
Pulse repetition rate (kHz)	15	0.05
Collimator aperture (mm)	100	80
Coupler aperture (mm)	80	300
Fiber diameter (μm)	10	1500
Fiber attenuation (dB/km)	0.02	30
Detector efficiency (%)	20	40
Dark count noise (Hz)	300	100

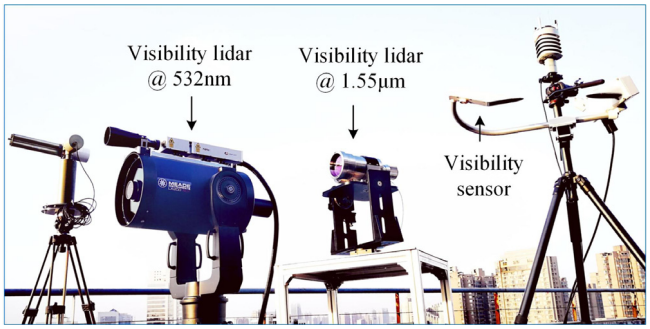

Fig. 2. Instruments used in the field experiments.

The 532 nm lidar is a mature system, which has been used for atmospheric detection for decades. A Mie scattering lidar system at 532 nm is built for observation of optical properties in the atmospheric boundary layer. The key parameters of two lidars are listed in Table 1. The 532 nm lidar has higher pulse energy and larger telescope than the 1.5 μm lidar.

The aerosol spectrometer (Grimm, 11-R) uses optical single particle detection for counting and classifying aerosol particles. It uses light source at a wavelength of 660 nm and measures the scattering light at 90°. It has 31 size channels with a particle detection size ranging from 0.25 to 32 μm. The temporal resolution of Grimm 11-R is 6 s. In this experiment, the raw data is averaged over 5 min.

The visibility sensor used in this experiment is a popular present weather detector (Vaisala, PWD50). The visibility sensor combines the functions of a forward scatter visibility meter, and evaluates visibility by measuring the intensity of infrared light scattered at a wavelength of 875 nm at an angle of 45°. The scatter measurement is converted to the visibility value, with an accuracy of ±10% at the 10 to 10 000 m range and ±20% at the 10 000 to 35 000 m range. Fig. 2 is a photo of the instruments used in the field experiments.

4. Field experiments and results

From 9:00 on April 21 to 9:00 on April 23, 2017, atmospheric visibility is detected at Hefei (31.83°N, 117.25°E) in Anhui province, China to demonstrate the new proposed algorithm. The location is 40 m above the sea level. The visibility can be calculated by using Eq. (11), and compares with the visibility measured by the Vaisala PWD50.

Raw lidar backscattering signal of 1.5 μm visibility lidar over 48 h is shown in Fig. 3(a). The lidar is emitted horizontally during the 48-h

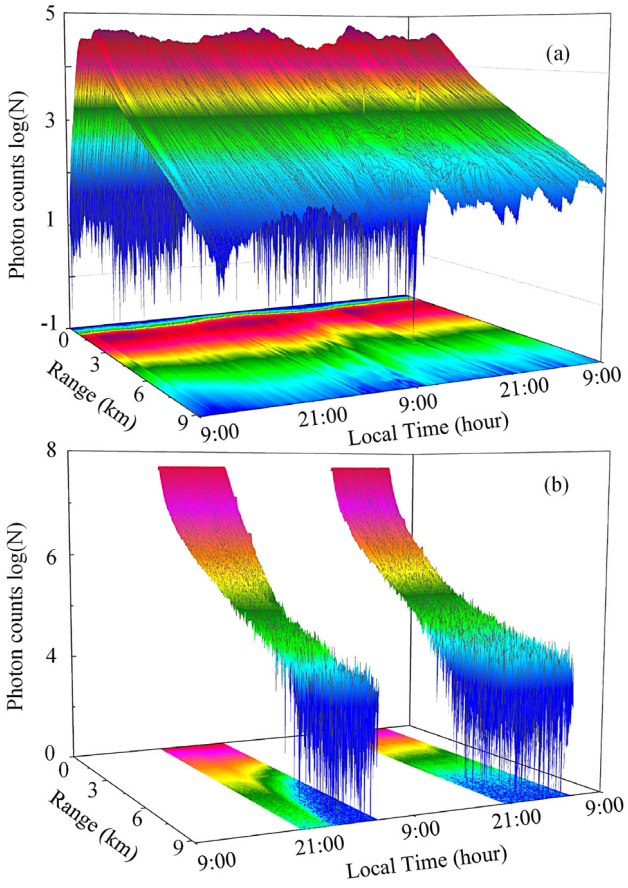

Fig. 3. Raw data of 1.55 μm lidar (a) and 532 nm lidar (b).

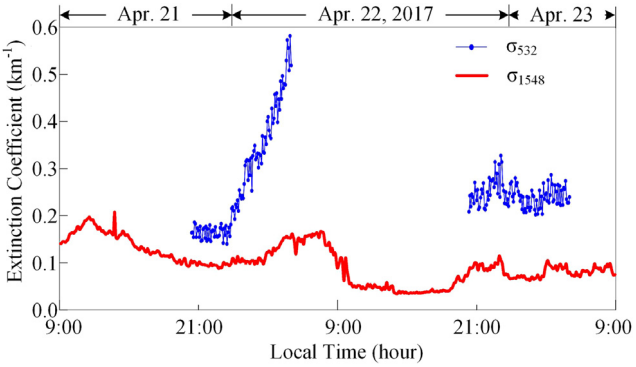

Fig. 4. The extinction coefficients of 1.55 μm lidar and 532 nm lidar.

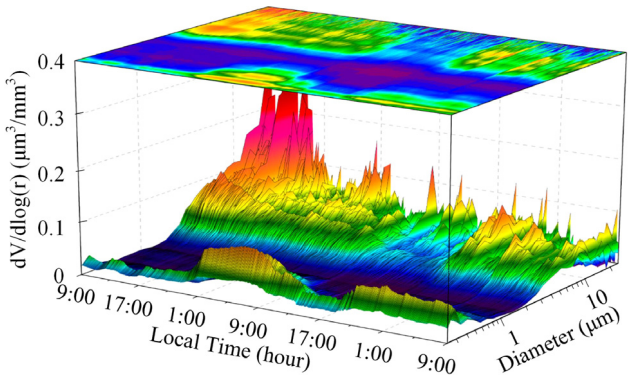

Fig. 5. Volume size distribution during 48 h.

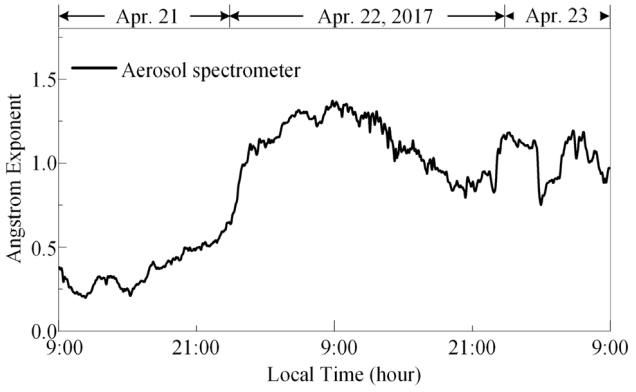

Fig. 6. The Angstrom wavelength exponent derived from aerosol spectrometer.

measurements. The temporal resolution and spatial resolution are set to 5 min and 45 m, respectively. Although the pulse energy is 110 μJ and the diameter of the telescope is only 80 mm, it can be seen in Fig. 3(a) that the signal can extend to 9 km horizontally. The pulse energy of the 532 nm lidar is 15 mJ, and the aperture of the telescope is 300 mm. As shown in Fig. 3(b), the raw backscattering signal at 532 nm lidar only extends to about 6 km horizontally. It is mainly due to the fact that, the extinction coefficient at 532 nm is larger than that at 1.5 μm for the same atmospheric conditions. Through the decaying speed of raw lidar signal at 532 nm, it is clear that the visibility during the first night changes fast, while it is relatively stable during the second night.

Since the visibility sensor is installed on the top of a building which is about 2 km far away from the lidars' location, the raw data from 1.5 km to 3 km are used to calculate extinction coefficients using Eq. (2). The range interval is shifted forward or backward with a maximum range of five hundred meters to make sure that the correlation coefficient of the linear fitting of Eq. (2) is greater than 0.95. The retrieved extinction coefficients at two wavelengths are plotted in Fig. 4. The raw data of lidars from 1 km to 9 km are used to calculate extinction coefficients using Eq. (2). In the two-day experiment, the value of σ_{1548} varies between 0.033 and 0.235 km^{-1}. While the values of σ_{532} varies between 0.132 and 0.585 km^{-1}, and between 0.203 and 0.328 km^{-1} for two nights, respectively. The σ_{532} is always larger than σ_{1548} throughout the experiment. A process of declining visibility is observed from 20:15, Apr. 21, 2017 to 4:55 next morning. Comparing the extinction coefficients at 20:15 and 4:55, the relative change of σ_{1548} is 57%, on the contrary, the relative change of σ_{532} is 246%.

The PSD is obtained from the aerosol spectrometer. To see changes of PSD more intuitively, we convert number distributions $n(r)$ to volume distributions by using Eq. (7). The volume distributions over 48 h are shown in Fig. 5. The fine mode and coarse mode have different trends. The change period of fine mode's volume distribution is 24 h and there are two peaks in the 48 h observation. It keeps lower than 0.03 $\mu m^3/mm^3$ from 9:00 on Apr. 21 to 21:00 on Apr. 21. Then it becomes larger over next 4 h and keeps higher than 0.05 $\mu m^3/mm^3$ till 9:00 on Apr. 21. The next day and the first day have almost the same variation. Generally, the amount of fine mode's particles rises from 21:00, then it keeps a larger value than daytime. However the coarse mode's volume distributions are affected by emergencies and less regular. From 9:00 on Apr. 21 to 17:00 on Apr. 21, a burst of coarse mode's particles is observed.

The Angstrom wavelength exponent for wavelengths 0.55 μm and 1.55 μm derived from aerosol spectrometer is shown in Fig. 6. The Angstrom wavelength exponent from aerosol spectrometer rises from 0.40 at 9:00, Apr. 21 to 1.31 at 9:00, Apr. 22. The Angstrom wavelength

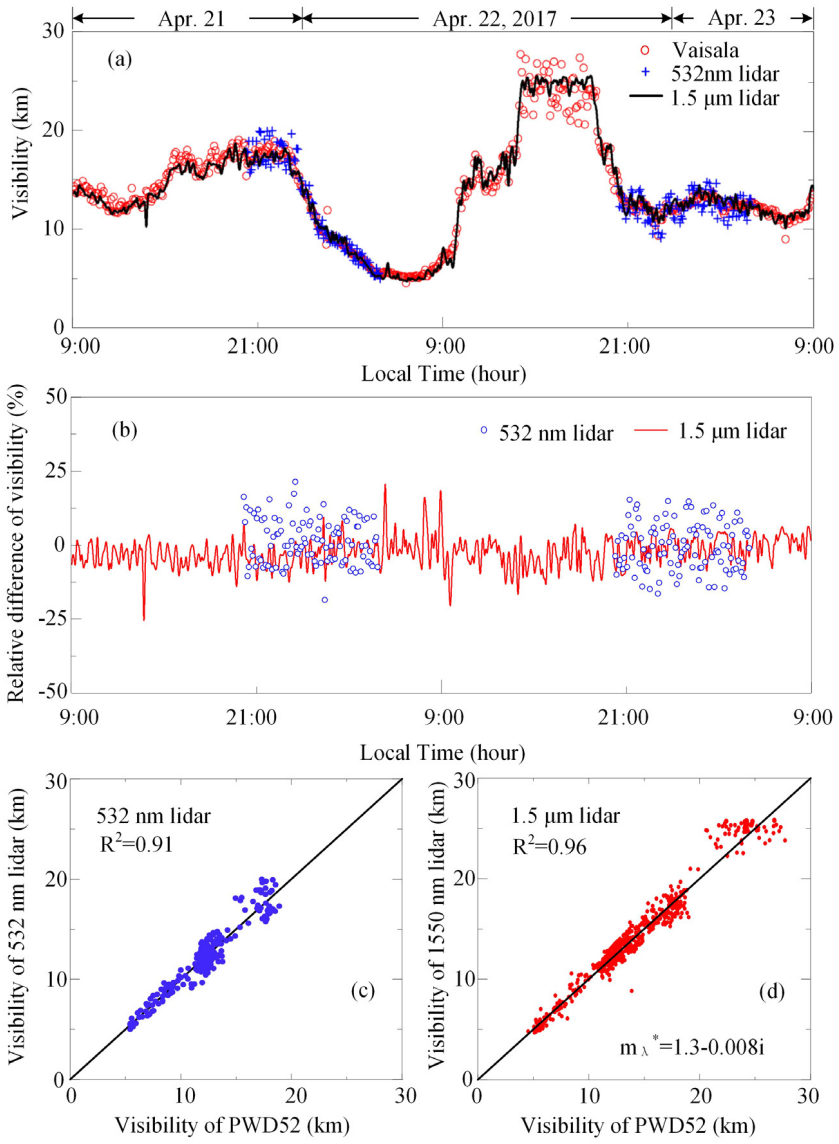

Fig. 7. Visibilities derived from different methods during 48 h (a), the relative difference of visibility measured by lidars and visibility sensor (b), comparison of visibilities based 532 nm lidar and PWD52 (c), comparison of visibilities based on 1.5 μm lidar and PWD52 (d)

exponent is smaller than 0.5 during the first 12 h since the air has a lot of coarse mode's particles (diameter bigger than 1 μm). Then it becomes larger and large due to the rise of fine mode's particles (diameter smaller than 1 μm).

The visibilities derived from 1.5 μm eye-safe visibility lidar using Eq. (11) and Vaisala PWD50 are shown in Fig. 7(a). The two segments of visibility measured by 532 nm visibility lidar are also shown in Fig. 7(a). As we can see from Fig. 7(a), visibility is 14.4 km when the experiment beginning. Then visibility rises to 17.9 km until 23:00, Apr. 21. Between 23:00, Apr. 21 and 8:00, Apr. 22, the visibility falls fast as the emergence of haze. Because of the evaporation of water, visibility rises to 25.9 km after the sunrise. In such a large dynamic range, the consistency of the 1.5 visibility lidar with visibility sensor is very good. It is obvious that the visibility of the second day is higher than the visibility at the same time of the previous day, because the particles' amounts of the second day are smaller than the first day, as shown in Fig. 5. It can be seen from Fig. 7(b) that the mean relative difference between the 1.5 μm lidar and Vaisala PWD50 is 5.2% with a standard deviation of 0.06. And the mean relative difference between the 532 nm lidar and visibility meter is 6.7% with a standard deviation of 0.08.

Errors in estimating the visibility at 532 nm during 48 h are shown in Fig. 7(c). The results are highly consistent between 532 nm lidar and visibility sensor with the *R*-square value of 0.91. Errors in estimating the visibility at 1.55 μm during 48 h are shown in Fig. 7(d) with the *R*-square value of 0.96. The complex refractive index is set to be 1.3–0.008i as an empirical value. It is obvious that, with the reference of in situ measurements from PWD50, considering in situ PSD can get an accurate result.

5. Conclusion

A method for the retrieval of visibility from 1.5 μm lidar combined with the measurements of aerosol spectrometer was proposed, which can adjust measures to local conditions. A compact micropulse aerosol lidar incorporating a fiber laser at 1.5 μm has been constructed in order to verify this method. A 532 nm lidar also has been constructed to compare the atmospheric extinction coefficient between 532 nm and 1.55 μm. And a Vaisala visibility sensor was used to validate our new model. Continuous observation of visibility was performed. In the comparison experiments, the average relative error between the retrieved visibility using our algorithm and visibility measured by visibility sensor is 5.2% with the *R*-square value of 0.96. If there is no significant pollution sources along the detection path, our lidar shows

good agreement with traditional visibility sensor during day and night. Since the is smaller than in mast atmospheric conditions, the 1.5 μm visibility lidar has further detection range than the 532 nm visibility lidar. More experiments in different air conditions, like fog or sandstorm weather will be done in the future to find the empirical relation of the temperature, relative humidity and the Angstrom exponent between 1.5 μm and 532 nm. We will also create a new iterative algorithm to calculate the extinction coefficient at 1.5 μm and the Angstrom exponent between 1.5 μm and 532 nm in different range, using the lidar's measurement and the PSD measured near lidar station.

References

[1] M.A. Delucchi, J.J. Murphy, D.R. McCubbin, The health and visibility cost of air pollution: a comparison of estimation methods, J. Environ. Manag. 64 (2002) 139–152.

[2] C. Weitkamp (Ed.), Lidar: Range-Resolved Optical Remote Sensing of the Atmosphere, Springer, 2005.

[3] J. Yin, Y. Cao, Y. Li, S. Liao, L. Zhang, J. Ren, W. Cai, W. Liu, B. Li, H. Dai, G. Li, Q. Lu, Y. Gong, Y. Xu, S. Li, F. Li, Y. Yin, Z. Jiang, X. Zhang, N. Wang, X. Chang, Z. Zhu, N. Liu, Y. Chen, C. Lu, R. Shu, C. Peng, J. Wang, J.W. Pan, Satellite-based entanglement distribution over 1200 kilometers, Science 356 (2017) 1140–1144.

[4] D. Baumer, B. Vogel, S. Versick, R. Rinke, O. Mhler, M. Schnaiter, Relationship of visibility, aerosol optical thickness and aerosol size distribution in an ageing air mass over South-West Germany, Atmos. Environ. 42 (2008) 989–998.

[5] S. Wu, X. Song, B. Liu, G. Dai, J. Liu, K. Zhang, S. Qin, D. Hua, F. Gao, L. Liu, Mobile multi-wavelength polarization Raman lidar for water vapor, cloud and aerosol measurement, Opt. Express 23 (2015) 33870–33892.

[6] I.G. McKendry, D. Van der Kamp, K.B. Strawbridge, A. Christen, B. Crawford, Simultaneous observations of boundary-layer aerosol layers with CL31 ceilometer and 1064/532 nm lidar, Atmos. Environ. 43 (2009) 5847–5852.

[7] H. Xia, D. Sun, Y. Yang, F. Shen, J. Dong, T. Kobayashi, Fabry–Perot interferometer based Mie Doppler lidar for low tropospheric wind observation, Appl. Opt. 46 (2007) 7120–7131.

[8] S.A. Lisenko, M.M. Kugeiko, V.V. Khomich, Multifrequency lidar sounding of air pollution by particulate matter with separation into respirable fractions, Atmos. Ocean. Opt. 29 (2016) 288–297.

[9] S.D. Mayor, S.M. Spuler, B.M. Morley, E. Loew, Polarization lidar at 1.54 microns and observations of plumes from aerosol generators, Opt. Eng. 46 (2007) 096201.

[10] S.F. De Wekker, S.D. Mayor, Observations of atmospheric structure and dynamics in the Owens Valley of California with a ground-based, eye-safe, scanning aerosol lidar, J. Appl. Meteorol. Climatol. 48 (2009) 1483–1499.

[11] S.D. Mayor, P. Drian, C.F. Mauzey, S.M. Spuler, P. Ponsardin, J. Pruitt, D. Ramsey, N.S. Higdon, Comparison of an analog direct detection and a micropulse aerosol lidar at 1.5-microns wavelength for wind field observations with first results over the ocean, J. Appl. Remote Sens. 10 (2016) 016031.

[12] O. Steinvall, R. Persson, F. Berglund, O. Gustafsson, J. Ohgren, F. Gustafsson, Using an eye-safe laser rangefinder to assist active and passive electro-optical sensor performance prediction in low visibility conditions, Opt. Eng. 54 (2015) 074103.

[13] J.D. Spinhirne, Micro pulse lidar, IEEE Trans. Geosci. Remote Sens. 31 (1) (1993) 48–55.

[14] H. Xia, G. Shentu, M. Shangguan, X. Xia, X. Jia, C. Wang, J. Zhang, J.S. Pelc, M.M. Fejer, Q. Zhang, X. Dou, J.W. Pan, Long-range micro-pulse aerosol lidar at 1.5 μm with an upconversion single-photon detector, Opt. Lett. 40 (2015) 1579–1582.

[15] Laser Institute of America, American National Standard for Safe Use of Lasers ANSI Z136.12007, American National Standards Institute, Inc., 2007.

[16] S.K. Liao, H.L. Yong, C. Liu, G.L. Shentu, D.D. Li, J. Lin, H. Dai, S.Q. Zhao, B. Li, J.Y. Guan, W. Chen, Y.H. Gong, Y. Li, Z.H. Lin, G.S. Pan, J.S. Pelc, M.M. Fejer, W.Z. Zhang, W.Y. Liu, J. Yin, J.G. Ren, X.B. Wang, Q. Zhang, C.Z. Peng, J.W. Pan, Long-distance free-space quantum key distribution in daylight towards inter-satellite communication, Nat. Photonics 11 (2017) nphoton.116.

[17] M. Shangguan, H. Xia, C. Wang, J. Qiu, G. Shentu, Q. Zhang, X. Dou, J. Pan, All-fiber upconversion high spectral resolution wind lidar using a Fabry–Perot interferometer, Opt. Express 24 (2016) 19322–19336.

[18] H. Xia, M. Shangguan, C. Wang, G. Shentu, J. Qiu, Q. Zhang, X. Dou, J.W. Pan, Micropulse upconversion Doppler lidar for wind and visibility detection in the atmospheric boundary layer, Opt. Lett. 41 (2016) 5218–5221.

[19] P.W. Kruse, L.D. McGlauchlin, R.B. McQuistan, Elements of Infrared Technology: Generation, Transmission and Detection, Jonh Wiley & Sons, New York, 1962 (Chapter 5).

[20] I.I. Kim, B. McArthur, E.J. Korevaar, Comparisorn of laser beam propagation at 785 nm and 1550 nm in fog and haze for optical wireless communications, Proc. SPIE 4214 (2001) 26–37.

[21] M. Al Naboulsi, H. Sizun, F. de Fornel, Fog attenuation prediction for optical and infrared waves, Opt. Eng. 43 (2004) 319–329.

[22] M. Grabner, V. Kvicera, The wavelength dependent model of extinction in fog and haze for free space optical communication, Opt. Express 19 (2011) 3379–3386.

[23] S. Grob, M. Esselborn, B. Weinzierl, M. Wirth, A. Fix, A. Petzold, Aerosol classification by airborne high spectral resolution lidar observations, Atmos. Chem. Phys. 13 (2013) 2487–2505.

[24] Q. He, C. Li, F. Geng, G. Zhou, W. Gao, W. Yu, Z. Li, M. Du, A parameterization scheme of aerosol vertical distribution for surface-level visibility retrieval from satellite remote sensing, Remote Sens. Environ. 181 (2016) 1–13.

[25] S. Liang, B. Zhong, H. Fang, Improved estimation of aerosol optical depth from MODIS imagery over land surfaces, Remote Sens. Environ. 104 (2006) 416–425.

[26] D. Doxaran, J.M. Froidefonrd, S. Lavender, P. Castaing, Spectral signature of highly turbid waters. Application with SPOT data to quantify suspended particulate matter concentrations, Remote Sens. Environ. 81 (2002) 149–161.

[27] M.D. Steven, The sensitivity of the OSAVI vegetation index to observational parameters, Remote Sens. Environ. 63 (1998) 49–60.

[28] W. Viezee, E.E. Uthe, R.T.H. Collis, Lidar observations of airfield approach conditions: an exploratory study, J. Appl. Meteorol. 8 (1969) 274–283.

[29] J.D. Klett, Stable analytical inversion solution for processing lidar returns, Appl. Opt. 20 (1981) 211–220.

[30] F.G. Fernald, Analysis of atmospheric lidar observations: some comments, Appl. Opt. 23 (1984) 652–653.

[31] H. Xia, X. Dou, D. Sun, Z. Shu, X. Xue, Y. Han, D. Hu, Y. Han, T. Cheng, Mid-altitude wind measurements with mobile Rayleigh Doppler lidar incorporating system-level optical frequency control method, Opt. Express 20 (2012) 15286–15300.

[32] NOAA, NASA and USAF, U.S. Standard Atmosphere, U.S. Government Printing Office, 1976.

[33] C. Yu, M. Shangguan, H. Xia, J. Zhang, X. Dou, J.W. Pan, Fully integrated free-running InGaAs/InP single-photon detector for accurate lidar applications, Opt. Express 25 (2017) 14611–14620.

[34] G.L. Shentu, J.S. Pelc, X.D. Wang, Q.C. Sun, M.Y. Zheng, M.M. Fejer, Q. Zhang, J.W. Pan, Ultralow noise up-conversion detector and spectrometer for the telecom band, Opt. Express 21 (2013) 13986–13991.

[35] H. Xia, M. Shangguan, G. Shentu, C. Wang, J. Qiu, M. Zheng, X. Xie, X. Dou, Q. Zhang, J.W. Pan, Brillouin optical time-domain reflectometry using up-conversion single-photon detector, Opt. Commun. 381 (2016) 37–42.